Biomaterials Science

ROYAL SOCIETY OF CHEMISTRY

PAPER

View Article Online
View Journal | View Issue

Cite this: *Biomater. Sci.*, 2023, **11**, 4583

Fabrication of polyvinyl pyrrolidone-K90/Eudragit RL100-based dissolving microneedle patches loaded with alpha-arbutin and resveratrol for skin depigmentation†

Nway Nway Aung,[a,b] Supusson Pengnam,[a] Tanasait Ngawhirunpat,[a] Theerasak Rojanarata,[a] Prasopchai Patrojanasophon,[a] Praneet Opanasopit[a] and Boonnada Pamornpathomkul *[a]

Alpha-arbutin (AA) and resveratrol (Res) are widely used in skin-lightening products. However, current topical formulations have minimal skin-lightening effects due to the low absorption and poor solubility of these active compounds. This study investigated the efficacy and safety of using dissolving microneedle (DMN) patches to improve the delivery of AA and Res for skin depigmentation. The DMN patches (F0–F3) fabricated from polyvinyl pyrrolidone-K90 (PVP-K90)/Eudragit RL100 blends successfully penetrated excised porcine skin and showed sufficient mechanical strength to resist compression forces. Loading DMNs with 10% AA and 2% Res at a ratio of 5 : 1 (F3) resulted in a synergistic interaction between the drugs with desirable dissolving ability, drug loading, and stability. Furthermore, both *in vitro* and *in vivo* studies revealed that the use of F3 DMN patches successfully enhanced the intradermal delivery of AA and Res over a 24 h period, with the delivered amount being higher (~2.6 times) than that provided by a cream formulation ($P < 0.05$). After removing the DMN patches, the mice's skin was spontaneously and completely resealed within 12 h. In clinical studies, F3 DMN patches slightly decreased the melanin index of the participants without causing skin irritation or erythema at any time during the 24 h period when the patches were applied ($P < 0.05$). Moreover, application of the patches for 24 h was not found to affect skin hydration, transepidermal water loss, or skin elasticity. Therefore, AA/Res-loaded DMN patches could offer a promising approach for the effective local delivery of cosmetic agents for skin depigmentation.

Received 25th January 2023,
Accepted 11th April 2023

DOI: 10.1039/d3bm00132f

rsc.li/biomaterials-science

1. Introduction

Skin pigmentation abnormalities are the third most common dermatological disorders in the world. During human evolution, the body adapted to higher ultraviolet radiation by increasing melanin production to protect the skin from damage. In contemporary societies, however, fair skin without dark spots has become an important ideal of female beauty, especially in Asia-Pacific countries. Fair skin is widely regarded as highly desirable for its beneficial effects on self-confidence, attractiveness, well-being, and beauty. The skincare lightening market has grown rapidly in recent years as consumers seek treatment for skin hyperpigmentation disorders, such as melasma, age spots, and solar lentigo.[1,2]

Melanin is a pigment synthesized by epidermal melanocytes through melanogenesis.[3] Skin depigmentation can be achieved by targeting different melanin metabolic pathways. The most widelyused approach is inhibiting the copper-containing tyrosinase enzyme in melanin biosynthesis.[4,5] Thus, many cosmetic industries have been investigating the best technology to achieve skin depigmentation using proven tyrosinase inhibitors, such as ascorbic acid, tranexamic acid, alpha-arbutin, resveratrol, niacinamide, aloesin, and kojic acid.

Some synthetic skin depigmentation treatments, such as hydroquinone and kojic acid, can cause skin irritation or acute dermatitis. In contrast, arbutin has been widely used because of its potent tyrosinase inhibitory activity and better safety profile. Arbutin is a hydroquinone naturally found in blueberry and cranberry plants and can exist as free, ether, or esterified forms such as alpha-arbutin and beta-arbutin.[6] Alpha-arbutin (AA) or 4-hydroxyphenyl alpha-glucopyranoside is the alpha-glycosylated form of arbutin.[7] AA reversibly inhibits tyrosinase

[a]*Pharmaceutical Development of Green Innovations Group (PDGIG), Faculty of Pharmacy, Silpakorn University, Nakhon Pathom, 73000, Thailand. E-mail: pamornpathomkul_b@su.ac.th; Tel: +66 34-255800*
[b]*Pharmaceutical Factory, Kyaukse, Myanmar*
† Electronic supplementary information (ESI) available. See DOI: https://doi.org/10.1039/d3bm00132f

and melanosome transfer due to its structural similarities to tyrosine, with ten times more potency than beta arbutin.[8] Therefore, AA has been of increasing interest for its use in various cutaneous hyperpigmentation treatments, due to the lack of significant adverse effects, compared with hydroquinone.[9,10] However, high AA concentrations (1–7% w/w) need to be applied to achieve skin lightening. This is due to the high hydrophilicity of AA, resulting in poor percutaneous absorption and restricted penetration into the stratum basale of the skin where melanocytes are located.[11]

Resveratrol (Res) (3,5,4′-trihydroxy-*trans*-stilbene) is a hydrophobic polyphenol composed of two aromatic rings connected by an ethylene bridge. It is found in food such as grapes, red wine, peanuts, and cocoa.[12] Res has been demonstrated to exhibit antioxidant, anticancer, anti-obesity, anti-proliferation, antiviral, and anti-inflammatory effects.[13–19] Recently, Res has been applied in cosmetology for its anti-aging properties. Res also exhibits hypopigmented effects directly or indirectly. In the direct pathway, Res can competitively inhibit tyrosinase. In the indirect pathway, Res can inhibit tyrosinase transcription or regulate it post-transcriptionally to regulate keratinocyte inflammation and protect keratinocytes from oxidative damage.[20–22] Previous works have shown a synergistic effect between antioxidant defense systems and melanogenesis, increasing the ability of antioxidants, such as Res, to reduce melanin production.[18] These suggest that Res can be used for melasma treatment by suppressing melanin formation and exerting systemic effects.[23] Although Res exhibits broad health benefits, its utilization in topical products is limited due to its chemical instability and poor solubility in conventional cosmetic formulations.[2] To overcome this, new modifying technologies, such as nanotechnology, lasers, electroporation, microdermabrasion, iontophoresis, gene gun, and microneedles, have been explored.[24,25]

The use of microneedle (MN) drug delivery systems has been proposed to be an effective and attractive method for pharmaceutical and cosmetic applications.[26,27] This novel technique is designed to be minimally invasive and painless.[28] MNs contain hundreds to thousands of needles 100 to 1500 μm in length, arranged in arrays on a patch. These create microchannels across the stratum corneum (SC) to transport drugs into the skin.[29,30] Among MNs, dissolving microneedles (DMNs) have gained the greatest interest. DMNs are drug-loaded biodegradable polymeric microstructures that dissolve upon contact with cutaneous interstitial fluid after insertion and can successfully deliver drugs without leaving biohazardous sharps. Furthermore, DMNs can be used to achieve the desired drug delivery rates by adjusting the degradation rate of the polymer used in the MN matrix.[31] DMNs revealed potential applications as a drug delivery system in different therapeutic areas. More recently, DMNs fabricated from PVP and polycaprolactone (PCL) were successfully applied as patches for the transdermal delivery of allopurinol in an *in vitro* and *in vivo* study with the purpose of acute hyperuricemia treatment.[32] Zeng *et al.* (2022) successfully developed as-fabricated flexible MN dressings loaded with metformin and CaO_2@polydopamine (CaO_2@PDA) nanoparticles for antibacterial properties against both *S. aureus* and *E. coli* and accelerated diabetic skin-wound healing.[33] Moreover, Ruan *et al.* (2021) reported that CaO_2@Mn-PDA nanoformulations embedded in MNs combined near-infrared light irradiation leading to the generation of a minimally invasive and synergistic therapeutic against skin melanoma.[34] Our previous study investigated DMN patches prepared using different polymers, including Gantrez™ S-97, hydroxypropyl methylcellulose (HPMC), PVP, chitosan, and their combinations. We found that 8% HPMC/PVP K-90 (1 : 1) DMN was optimal for AA delivery.[35] Moreover, we developed AA-loaded polyacrylic acid-*co*-maleic acid and polyvinyl alcohol (PVA) (1 : 4) DMNs and hydrogel-forming microneedles (HMNs). We found that AA-loaded DMNs significantly enhanced AA permeation *in vitro* and *in vivo* compared to AA-loaded HMNs.

Previous studies suggest overlapping and distinct mechanisms by which AA and Res result in depigmenting effects. Whether there is a synergistic effect between them is a question worth exploring. Therefore, this study aims to study the synergistic effects of AA and Res in promoting skin depigmentation using a drug delivery platform to overcome the limitations of these drugs. To utilize the benefits that the DMN platform provides, DMN patches incorporating AA and Res were developed. AA/Res-loaded DMN patches were fabricated from biodegradable polymer blends of Eudragit RL 100 and PVP-K90 and their morphology, mechanical strength, drug contents, *ex vivo* and *in vivo* dissolutions, *in vitro* and *in vivo* skin permeation and accumulation, *in vivo* skin resealing, and clinical application were assessed.

2. Materials and methods

2.1. Materials

AA (MW = 272.25 g mol^{-1}), Res (MW = 228.24 g mol^{-1}), PVP-K90 (MW = 360 kDa), kojic acid, α-melanocyte-stimulating hormone (α-MSH), melanin, and methyl thiazolydiphenyl-tetrazoline bromide (MTT) were purchased from Sigma-Aldrich, MO, USA. Eudragit RL100 (MW = 32 000 g mol^{-1}) was obtained from Evonik Röhm GmbH, Germany. Dimethyl sulfoxide (DMSO) was obtained from EuroClone S.p.A. (Milan, Italy). Dulbecco's modified Eagle's medium (DMEM) was obtained from Gibco BRL, MD, USA. Fetal bovine serum (FBS), 1% penicillin/streptomycin, and Triton X-100 were acquired from AMRESCO (OH, USA). All reagents and solvents used were of analytical grade.

2.2. Cell culture

B16F10 mouse melanoma cells were obtained from the American Type Culture Collection and cultured in RPMI 1640 medium supplemented with 10% FBS and 1% penicillin/streptomycin. Cells were incubated at 37 °C with 5% CO_2 in a humidified environment for three days. After incubation, the culture medium was replaced with DMEM with α-MSH for all experiments.

2.3. Cell viability assay

The cytotoxic activities of AA and Res on B16F10 melanoma cells were determined using the MTT assay. Cells were seeded in 96-well plates at a density of 0.3×10^4 cells per well and incubated at 37 °C with 5% CO_2. After 24 h, α-MSH-induced cells were treated with various concentrations of AA (10–4000 μg mL^{-1}) or Res (5–50 μg mL^{-1}) for 48 h. The medium was carefully removed and the cells were washed with PBS. To each well, 25 μL of MTT solution (0.5 mg mL^{-1}) and 100 μL of the fresh medium (DMEM) were added. After 3 h of incubation, the MTT solution was replaced with 100 μL DMSO to dissolve formazan crystals. The absorbance of each sample was measured at 550 nm using a microplate reader (VICTOR® Nivo™ Multimode Plate Reader, PerkinElmer, Germany). Percent cell viability was calculated using eqn (1), with untreated cells serving as reference controls.[36]

$$\%\,\text{Cell viability} = \frac{\text{Absorbance of sample}}{\text{Absorbance of control}} \times 100 \quad (1)$$

2.4. Melanin content assay

The effects of AA and Res on melanin content were determined according to the method previously reported by Lim *et al.*[37] B16F10 melanoma cells were cultured in a 24-well plate at 1×10^5 cells per well at 37 °C with 5% CO_2 for 24 h. Cells were stimulated with α-MSH (100 μM) and treated with different doses of test compounds (100–2000 μg mL^{-1} of AA or 5–20 μg mL^{-1} of Res). Kojic acid (60 μg mL^{-1}) was used as a positive control. After 48 h of incubation, cells were harvested using trypsin and the resulting cell suspension was transferred from each well into a 1.5 mL Eppendorf tube. Cells were centrifuged at 3000*g* for 10 min. The supernatant was removed and the cells in the pellet were solubilized in 1 N NaOH/10% DMSO at 80 °C for 1 h. Cells were lysed and the supernatant was transferred into 96-well plates. The absorbance of each sample was measured at 405 nm using a microplate reader. Melanin levels in the samples were calculated using a standard curve obtained using solutions of synthetic melanin.

2.5. Synergism analysis of AA and Res

Drug synergism was evaluated based on the combination index (CI) theorem of Chou Talay.[38] The synergistic effect of AA and Res was determined using a non-constant ratio experiment followed by the melanin content assay mentioned above. For this experiment, exponentially growing B16F10 melanoma cells were exposed to a combination of varying AA concentrations (500–3000 μg mL^{-1}) with a fixed Res concentration (20 μg mL^{-1}) or a fixed AA concentration (2000 μg mL^{-1}) with varying concentrations of Res (5–30 μg mL^{-1}) for 48 h. Percent melanin content inhibition was obtained for all treatment combinations and the interaction effect was calculated using CompuSyn software (Version 1.0). The percentage of melanin content inhibition was converted to fraction affected (Fa) using eqn (2). The treatment concentration (μg mL^{-1}) and Fa were input into the software to calculate the CI value. CI values indicate the interaction between two drugs, where CI = 1, CI < 1, and CI > 1 represent additive, synergistic, or antagonistic interactions, respectively. The combination of the synergistic effect and low cell toxicity was selected for loading AA and Res into DMN formulations.[39]

$$\text{Fraction affected (Fa)} = \frac{\%\,\text{melanin contents inhibition}}{100} \quad (2)$$

2.6. Fabrication of unloaded DMN patches

A polymer blend solution of 14% w/w Eudragit RL 100 and 40% w/w PVP-K90 at a weight ratio of 1 : 2 was prepared according to our previous method.[40] Fabrication of unloaded and AA/Res-loaded DMN patches was achieved using micromolding. The prepared polymer blend was cast (0.67 g) onto laser-engineered silicone micromold templates without any drug loading. The silicone micromold was an array of 121 (11 × 11) cone-shaped needles that were 600 μm in height, 300 μm in width, and spaced 300 μm apart on a patch area of approximately 1 cm^2. The cast micromold was centrifuged (3500 rpm for 20 min) to eliminate air bubbles and push the polymer solutions into the bottom of the microholes. The fabricated DMN patches were dried at 25 °C for 48 h. Finally, the DMN patches were gently peeled off from each micromold.

2.7. Fabrication of AA/Res-loaded DMN patches

Four concentrations of AA and Res were used to fabricate AA/Res-loaded DMN patches while maintaining the AA : Res ratio fixed at 5 : 1, which exhibited a synergistic effect with low cell toxicity in previous experiments (section 2.5). The AA and Res concentrations used were designated as F0 (no active substances), F1 (2.5 : 0.5), F2 (5 : 1), F3 (10 : 2), and F4 (15 : 3). AA was dissolved in PVP-K90 solution (40% w/w), while Res was mixed with 14% w/w of Eudragit RL solution to enhance their solubilities. The resulting drug-loaded polymer solutions were combined to obtain a 1 : 2 mixture of 14% w/w Eudragit RL : 40% w/w PVP-K90. These formulations were used to fabricate DMN patches using the same process as the unloaded DMN patches. The AA/Res-loaded DMN patches were peeled off from the micromolds and stored in a desiccator until use.

2.8. Preparation of AA/Res-loaded physical mixtures or cream formulations

The amount of AA and Res loaded into a physical mixture and cream formulation was the same as that used in the optimal DMN patches (F3) that resulted in the highest skin permeation *in vitro*. To prepare a physical mixture, 10% AA (67 mg) was dissolved in 40% w/w PVP-K90 solution and 2% Res (13.4 mg) was dissolved in 14% w/w Eudragit RL solution. The solutions were combined and mixed until a homogeneous state was achieved. A combination cream formulation containing 10% AA and 2% Res was incorporated into a cream base (Siriraj Hospital®) and mixed until a homogeneous mixture was obtained.

2.9. Characterization of DMN patches

2.9.1. Morphological analysis of DMN patches. The morphology of the resulting DMN patches from each formulation was analyzed under a Dino-Lite microscope (AM 7915 series, Hsinchu, Taiwan). The optimal formulation was confirmed using a scanning electron microscope (SEM, Mixa TC, Czech Republic). A beam voltage of 5.0 kV was used to image the samples.

2.9.2. Loading efficiency and loading capacity of DMN patches. To evaluate the quantity of drug loaded into the DMN patches, each formulation of the DMN patches (F1 to F4) was separately weighed and dissolved in 10 mL PBS : methanol (1 : 1) for 6 h. Each sample solution was transferred into an Ultra filter (Amicon®, MW cut-off < 3 kDa) and centrifuged at 14 000*g* for 20 min to filter the polymer. The resulting solution was collected and analyzed using HPLC. The percentage loading efficiency and loading capacity of F1–F4 DMN patches were calculated using eqn (3) and (4), respectively.[41]

$$\%\,\text{Loading efficiency} = \frac{\text{Amount of drug(mg)}}{\text{Initial amount of drug(mg)}} \times 100 \quad (3)$$

$$\%\,\text{Loading capacity} = \frac{\text{Amount of drug(mg)}}{\text{Amount of polymer(mg)}} \times 100 \quad (4)$$

2.9.3. Mechanical strength of DMN patches. A mechanical strength study was performed to determine the optimal DMN patch formulation that can resist mechanical forces. Following our previous publication, vertical compression forces (3.388 N, 6.665 N, 10.769 N, and 13.31 N) were applied to each formulation patch using a Texture Analyzer (TA-XT, Stable Micro System Haslemere, UK). A pretest and post-test speed of 1 mm s^{-1} and a trigger force of 0.049 N were employed.[40] The patch height in the pretest (H_1) and post-test (H_2) was measured by using a Dino-Lite microscope. The percent reduction in the height of needles was calculated using eqn (5).[42–44]

$$\%\,\text{Reduction of needle height} = \frac{[H_1 - H_2]}{H_1} \times 100 \quad (5)$$

The successive increase in the application force caused deformation or breakage in the MNs, and the stage was withdrawn at several points during the test to understand the failure mode of MNs. Therefore, the force–displacement curve was also observed.[45] A texture analyzer connected with a 5 kg load cell was used to determine the mechanical strength of the MNs' compression mode. Briefly, before testing, MN patches were gently attached to a 1 cm cylinder stainless probe (P/1KSS) in the downward direction. The stainless probe was moved downward to a flat stainless steel at a speed of 1 mm s^{-1} and the force was continuously increased until a displacement of 0.6 mm was reached. Then, the stainless probe was moved upward at a speed of 1 mm s^{-1}. The force *versus* displacement curves were plotted.

2.9.4. *Ex vivo* skin insertion study of DMN patches. Neonatal porcine skin was used to model human skin for evaluating the extent of DMN patch insertion into the skin.[46] The skin was washed with PBS (pH 7.4) and the subcutaneous layer was removed. The skin was placed on a wax sheet with the dermis facing downward. Each DMN formulation patch was inserted into the porcine skin by applying pressure using the thumb for 30 seconds. To visualize the insertion holes at the patch application site, 1% methylene blue was loaded onto the applied site for 5 min. PBS solution was then used to wash out excess methylene blue and the skin surface was dried using tissue paper (Delicate Task Wipers, Kimtech). Holes on the punctured skin surface that stained blue were counted under a digital microscope. The percentage of stained microholes was calculated using eqn (6).

$$\%\,\text{Microholes appeared} = \frac{\text{Number of microholes appeared}}{\text{Number of needles per patch(121 needles)}} \times 100 \quad (6)$$

2.9.5. Insertion depth of DMN patches. Parafilm® M (126 ± 7 μm thickness) was used as a validated biological tissue model for MN insertion experiments, as described previously.[47] DMN patches were applied perpendicularly into an eight-sheet PF laminate (~1 mm in total thickness) using the Texture Analyser with a speed of 0.5 mm s^{-1} and an exerted force of 10.769 N per patch for 30 s. DMNs were then carefully removed from the PF, the sheets were unfolded and the number of holes created in each layer was counted using a digital microscope.

2.10. Dissolution study of DMN patches

2.10.1. *Ex vivo* dissolution study. Neonatal porcine skin was prepared as described in the previous section and allowed to saturate in PBS (pH 7.4) for 1 h. To estimate the *ex vivo* dissolution time of the needles of the DMN patches, DMNs were inserted into neonatal porcine skin at 32 °C. After 5, 10, 15, 30, or 45 min, the patches were removed from the skin and then visualized under a Dino-Lite microscope.[43]

2.10.2. *In vivo* dissolution study. ICR mice (female, 8-week old, 20–25 g) used in this study were obtained from the National Laboratory Animal Center, Mahidol University, Thailand. All animal procedures were performed in accordance with the Guidelines for Care and Use of Laboratory Animals of Silpakorn University and approved by the Animal Ethics Committee of the Faculty of Pharmacy, Silpakorn University (U1-08575-2563). Mice were acclimatized under laboratory conditions for 1 week. The hair on the abdominal area of each animal was shaved with an electric razor. Mice were then anesthetized by intraperitoneal injection of Zoletil® 100 (tiletamine and zolazepam) (50–80 mg kg^{-1}) and xylazine (8–16 mg kg^{-1}). AA/Res-loaded DMN patches were applied to the ventral skin. The application site was fixed with an occlusive film (Tegaderm™). The DMN patches were removed after 5, 10, or 15 min. Changes in the needle height were observed under a Dino-Lite microscope.[35]

2.11. Fourier transform infrared spectroscopy (FTIR)

To identify and characterize the interactions between the polymers and drugs, the FTIR spectra of PVP K-90 powder,

Eudragit RL powder, AA powder, Res powder, unloaded DMNs, and AA/Res-loaded DMNs were recorded using the attenuated total reflectance technique for the determination of functional groups. Nicolet iS5 (diamond crystal, Thermo Electron Corporation, USA), equipped with data analysis software, was used with a scanning range of 4000 to 500 cm^{-1} and a resolution of 4.0 cm^{-1}. Spectra were collected at an average of 16 scans.

2.12. Stability study

To investigate the stability of AA and Res loaded into the DMN patches, 10% AA and 2% Res-loaded DMN patches (F3) were kept at 25 °C ± 2 °C and 60% ± 5% relative humidity (RH) for 6 months under sealed and unsealed conditions. The physical and chemical stabilities of both groups were evaluated at 0, 1, 2, 3, and 6 months. Extraction of AA and Res was performed following the methods in section 2.9.2 (Loading efficiency and loading capacity of DMN patches) while percentage recovery was determined using the methods in section 2.15 (Quantitative analysis of AA and Res).[44]

2.13. *In vitro* skin permeation and accumulation study

The amounts of AA and Res permeated across the porcine skin after applying 10% AA and 2% Res-loaded DMN patches (F3), the AA/Res-loaded physical mixture, and cream formulations were studied using vertical Franz diffusion cells. The integrity of the neonatal porcine skin samples was assessed using an electrical resistance method. The skin was ascertained to be intact before being used in the study. Skin permeation was performed over 24 h by placing the porcine skin on a receptor chamber filled with PBS (pH 7.4) as a mimic physiological medium, maintained at 32 °C and stirred continuously. DMN patches were inserted into the skin using thumb pressure for 30 s and secured with a metal block. The physical mixture and cream formulations were loaded with equal quantities of the drugs as the DMN patches and applied to the porcine skin topically. The sample solutions (500 μl) were withdrawn from the receptor compartment at predefined time points (1, 2, 4, 6, 8, 12, and 24 h) after which they were refilled with an equal amount of fresh PBS. The amount of AA and Res that permeated into the skin was analyzed using HPLC. The cumulative permeation amount of AA and Res through a Franz diffusion cell per unit area of the porcine skin (μg cm^{-2}) was plotted against time (n = 3). In addition, the flux value of drug permeability was calculated from the slope of the linear portion of the permeation profile.[48]

At the end of the skin permeation study, the amount of AA and Res accumulated in the skin layer was evaluated. The residual drug on the porcine skin was removed with PBS. A 1 cm^2 skin area where the patches were applied was cut and sliced into small pieces. To extract the active compounds from the skin, acetonitrile : water (0.1 : 1) was added into the sample and the mixture was vortexed for 1 h. The sample was centrifuged at 14 000*g* for 20 min. The supernatant was collected and analyzed using HPLC.

2.14. *In vivo* permeation study

An animal study was carried out to evaluate the permeation of AA and Res *in vivo*. ICR mice were obtained and acclimatized as described in section 2.10.2. Mice were separated into two groups (n = 6): the first group received 10% AA and 2% Res-loaded DMN patches (F3) and the second group received 10% AA and 2% Res combination cream. The AA/Res-loaded DMN patches were manually applied to the abdominal skin and kept in place for 24 h. For the second group, a 3 mm circular hole was punched through Microfoam® tape (3M, Thailand) with a thickness of 1 mm. The punched tape was attached to the skin and the AA/Res-loaded cream formulation was applied into the holes and left for 24 h. The DMN patches and cream formulations were covered with the Tegaderm™ occlusive film to prevent removal. At the end of the experiment, treatment formulations that remained were removed from the skin. The skins where DMN patches were applied were cut and prepared as previously described in section 2.13. Blood samples were also collected through cardiac puncture after the mice had been euthanized with diethyl ether. The blood samples collected from the mice were centrifuged at 15 000*g* at 4 °C for 15 min to precipitate the plasma. The levels of AA and Res in the plasma and skin were measured using HPLC.

2.15. Quantitative analysis of AA and Res

Quantification of AA and Res was performed separately using HPLC (Agilent 1269 series, Waldbronn, Germany) with a UV visible detector. Separations were performed in a C18 column (VertiSep® GES 250 × 4.6 mm, 5 μm, Thermo Fisher, MA, USA), with an injection volume of 25 μL. To quantify AA, water : methanol (92 : 8, v/v) was used as the mobile phase at a flow rate of 0.6 mL min^{-1}. The detector wavelength and the retention time were 280 nm and 11 min, respectively. To quantify Res, water : methanol (60 : 40, v/v) was used as the mobile phase at a flow rate of 1 mL min^{-1}. The detector wavelength and the retention time were 308 nm and 12 min, respectively.

2.16. *In vivo* skin resealing ability following application of DMN patches

A new set of mice were acclimatized and used in experiments to evaluate *in vivo* skin resealing following the removal of the AA/Res-loaded DMN patches. The AA/Res-loaded DMN patches (F3) were manually inserted into the abdominal skin of mice and left in place for 2.5 h. To observe how the microholes healed at the insertion site, 200 μL of methylene blue solution was applied to the DMN site following the removal of the patches at designated time points (0, 1, 2, 4, 8, and 12 h). PBS was used to wash off excess methylene blue solution. Skin recovery was imaged under a Dino-Lite microscope.[49]

2.17. Human studies

2.17.1. Human participants and study approval. All experiments were performed in accordance with the Guidelines of Good Clinical Practice and the International Council on Harmonization of Technical Requirements for Registration of

Pharmaceuticals for Human Use (ICH), and the experiments were approved by the ethics committee at Silpakorn University (COE 64.0705-088). Fifteen healthy volunteers (twelve women and three men) were included in this study. Informed consent was obtained from human participants of this study. All participants met the inclusion criteria which were being healthy and between the ages of 25 and 40. Exclusion criteria were pregnancy, a medical history of any active skin sensitivity, skin diseases, or the presence of damaged skin around the test sites. Prior to their participation in the study, all volunteers were provided with the information required by the protocol, which included the terms and conditions of the clinical test and an informed consent form. Participants were not permitted to apply moisturizing lotion or body powder 12 h before the start of the experiment for the duration of the study. Before the experimental procedures, all participants were instructed to rest in temperature-controlled rooms (25 °C ± 2 °C at 30%–50% humidity) for 10 min. DMN patches used in this study were sterilized under a UV lamp for 15 min.

2.17.2. Skin melanin, skin erythema, skin hydration, skin elasticity, transepidermal water loss (TEWL), and safety assessment. The forearm of each participant was used as the test site and wiped cleaned with 70% ethanol. Before DMN patch application, the test site was marked with a skin marker and used as a control. The levels of skin melanin, erythema, skin hydration, skin elasticity, and transepidermal water loss (TEWL) were measured using the DermaLab Combo® (SkinLab Combo, Cortex Technologies, Hadsund, Denmark) following the method of Tansathien *et al.* (2021).[50] An AA/Res-loaded DMN patch was applied to the test site using thumb pressure for 30 s and covered with a waterproof adhesive film to prevent the patch from slipping off the skin. After 24 h, the patch was carefully removed from the skin of each participant. The levels of skin melanin, skin erythema, skin hydration, skin elasticity, and TWEL were re-evaluated and compared with the control (the same area before the DMN patch was applied).[50] The environmental conditions, including light (500 lux), temperature (25 °C ± 2 °C), and humidity (30%–50%) at the time of the assessments were controlled to ensure the precision of the results. Signs of any skin abnormality following the removal of the DMN patches were also evaluated by physical examination and skin observation using a Dino-Lite Edge/5 MP digital microscope, AM 7915 series (Hsinchu, Taiwan).[51,52]

The percentage pigmentation level change was calculated relative to normal skin (skin pigmentation before the DMN patch was applied) using eqn (7). The percentage melanin index was then calculated with melanin of normal skin equated to 100% using eqn (8).[53]

$$\Delta\,\text{Melanin content}(\%) = \frac{M_{\text{After}} - M_{\text{Before}}}{M_{\text{Before}}} \times 100 \quad (7)$$

$$\%\text{Melanin index} = 100 + \Delta\text{melanin content}\ (\%) \quad (8)$$

Similarly, the change in skin erythema was calculated as the percentage erythema index (%EI) relative to the normal skin (skin vascularity measurement before the application of the DMN patch). The percentage erythema index was calculated with the vascularity of normal skin equated to 100% using eqn (9) and (10).

$$\Delta\,\text{Erythema level}(\%) = \frac{E_{\text{After}} - E_{\text{Before}}}{E_{\text{Before}}} \times 100 \quad (9)$$

$$\%\text{Erythema index} = 100 + \Delta\text{erythema level}\ (\%) \quad (10)$$

In the case of skin hydration, the percentage change and the skin hydration index were calculated using the same calculations for the melanin index and the erythema index.

2.18. Statistical analysis

All measurements were done in triplicate. The data are presented as mean and standard deviation (SD). The measured outcomes across treatment groups were compared using one-way analysis of variance. Two-tailed *P*-values < 0.05 were considered statistically significant.

3. Results and discussion

3.1. Effect of AA or Res on cell viability

The effects of AA and Res on B16F10 cell viability determined using the MTT assay are shown in Fig. 1A and B, respectively. The number of viable cells was more than 80% at AA concentrations of 10–2000 μg mL^{-1}, indicating no cytotoxicity at these doses. However, cytotoxic effects were observed in cells treated with 3000 and 4000 μg mL^{-1} AA (Fig. 1A). Res treatment resulted in more than 80% viability at 5–20 μg mL^{-1} (Fig. 1B). However, the percentage of viable cells significantly decreased when at higher Res concentrations of 25 and 50 μg mL^{-1}. These data indicate that higher concentrations of these compounds decreased viability in B16F10 cells.

3.2. Effect of AA and Res on the levels of melanin content

Besides melanocyte cytotoxic activities, the effect of test drugs on melanin content is also a critical factor in determining skin-lightening potential. The amount of melanin in B16F10 melanoma cells treated with AA or Res was determined and compared with the untreated control (no α-MSH induction, no drug treatment), negative control (with α-MSH induction; no drug treatment), and positive control (kojic acid-treated) groups. Melanin production increased in α-MSH-treated cells by approximately 21% compared to the untreated group ($P < 0.05$), as shown in Fig. s1A and s1B.† Upon exposure to different concentrations of AA or Res, melanin levels significantly decreased in a dose-dependent manner ($P < 0.01$). Additionally, 2000 μg mL^{-1} AA and 20 μg mL^{-1} Res inhibited α-MSH-induced melanin synthesis by more than 50%, similar to kojic acid (60 μg mL^{-1}). Therefore, 2000 μg mL^{-1} AA and 20 μg mL^{-1} Res were used in the succeeding experiments, as they showed no cytotoxicity and were effective at inhibiting melanin.

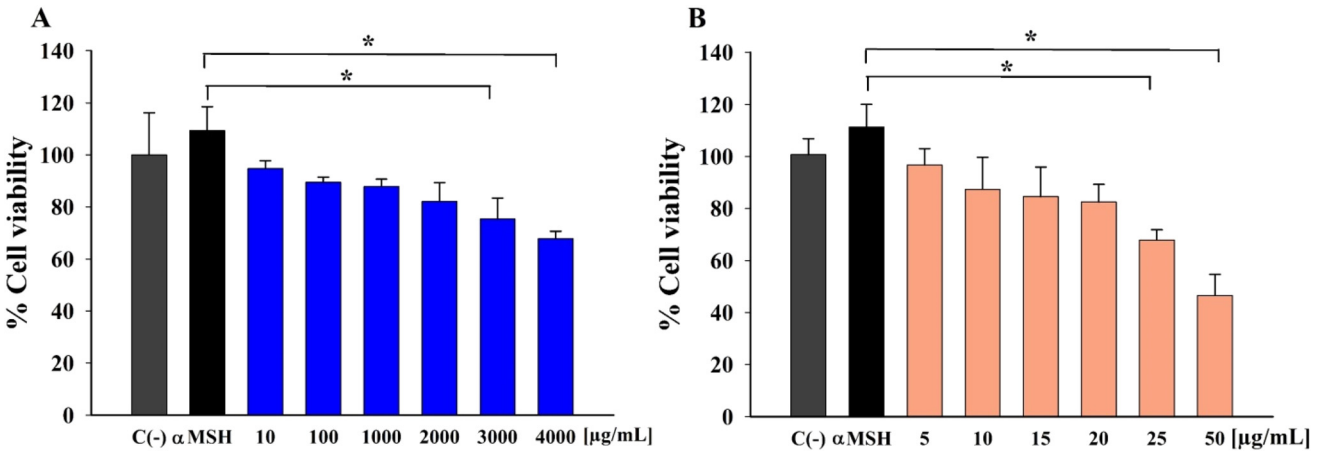

Fig. 1 Effects of different concentrations of (A) AA and (B) Res on B16F10 melanoma cell viability following induction with α-MSH (*$P < 0.05$, $n = 3$).

3.3. Combined treatment with non-constant AA and Res concentration ratios

Fig. 2A and B illustrate the percentage melanin content upon treatment with AA alone (500–3000 μg mL^{-1}), Res alone (5–30 μg mL^{-1}), and the combination of different concentrations of AA and Res (with 20 μg mL^{-1} Res or 2000 μg mL^{-1} AA, respectively) for 48 h. All treatment combinations exhibited a concentration-dependent inhibitory effect on B16F10 cell growth. Moreover, all combined treatments resulted in lower melanin contents than with AA or Res alone. These results suggest that combining AA and Res results in more potent inhibition of melanogenesis in B16F10 melanoma cells than when used individually.

3.4. Synergistic effect analysis

The combination index (CI) value was analyzed using CompuSyn software to determine the synergistic or antagonistic effects of different AA and Res combinations. The CI values of drug mixtures from melanin contents are summarized in Table s1.† Most drug combinations showed a synergistic effect (CI value < 1). This effect was concentration-dependent, with CI decreasing with increasing AA : Res ratios. In contrast, a 1 : 1 AA : Res ratio resulted in an additive interaction (CI value ~ 1). An AA : Res ratio of 5 : 1 (100 μg mL^{-1} AA combined with 20 μg mL^{-1} Res) decreased the melanin content by half compared to AA alone and exhibited a synergistic effect (CI = 0.85). Hence, this was selected for DMN fabrication and further evaluation.[39]

3.5. Characterization of DMN patches

3.5.1. Morphological analysis. In this study, the composite DMN patches fabricated using Eudragit RL and PVP-K90 were loaded with the synergistic AA : Res ratio of 5 : 1. The fabricated DMN patches were composed of 121 (11 × 11) needles. All the conical-shaped needles of the DMN patches were fully formed with a suitable geometry (575 ± 2.98 μm in height and 289 ± 1.21 μm in width), with a sharp and elegant appearance, on a 1 cm^2 patch area. The F0, F1, F2, and F3 DMN patches were

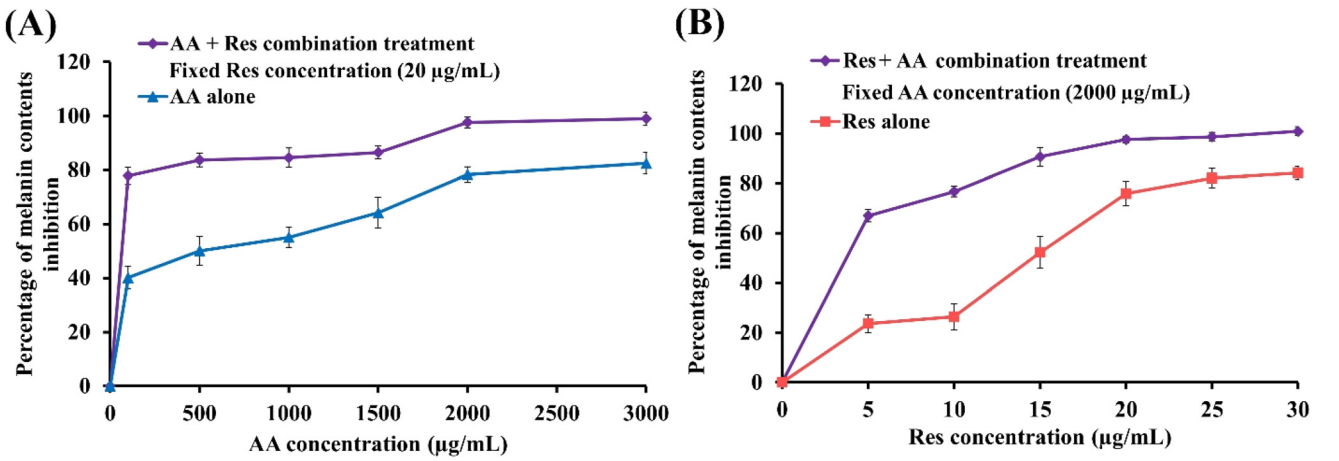

Fig. 2 Percentage melanin inhibition in B16F10 melanoma cells after treatment with (A) AA alone or AA and Res treatment combination, at a fixed Res concentration of 20 μg mL^{-1} and (B) Res alone or Res and AA treatment combination, at a fixed AA concentration of 2000 μg mL^{-1}. ($n = 3$).

durable, whereas the F4 DMN patches were fragile due to the high drug content in the formulation. SEM was used to observe the needles of the optimal DMN formulation (F3), as shown in Fig. 3.

3.5.2. Mechanical strength of DMN patches. The mechanical resistance of DMN patches to vertical compression forces of 3.388 N, 6.655 N, 10.769 N, and 13.31 N per patch applied for 30 s was measured to confirm the capability of DMN

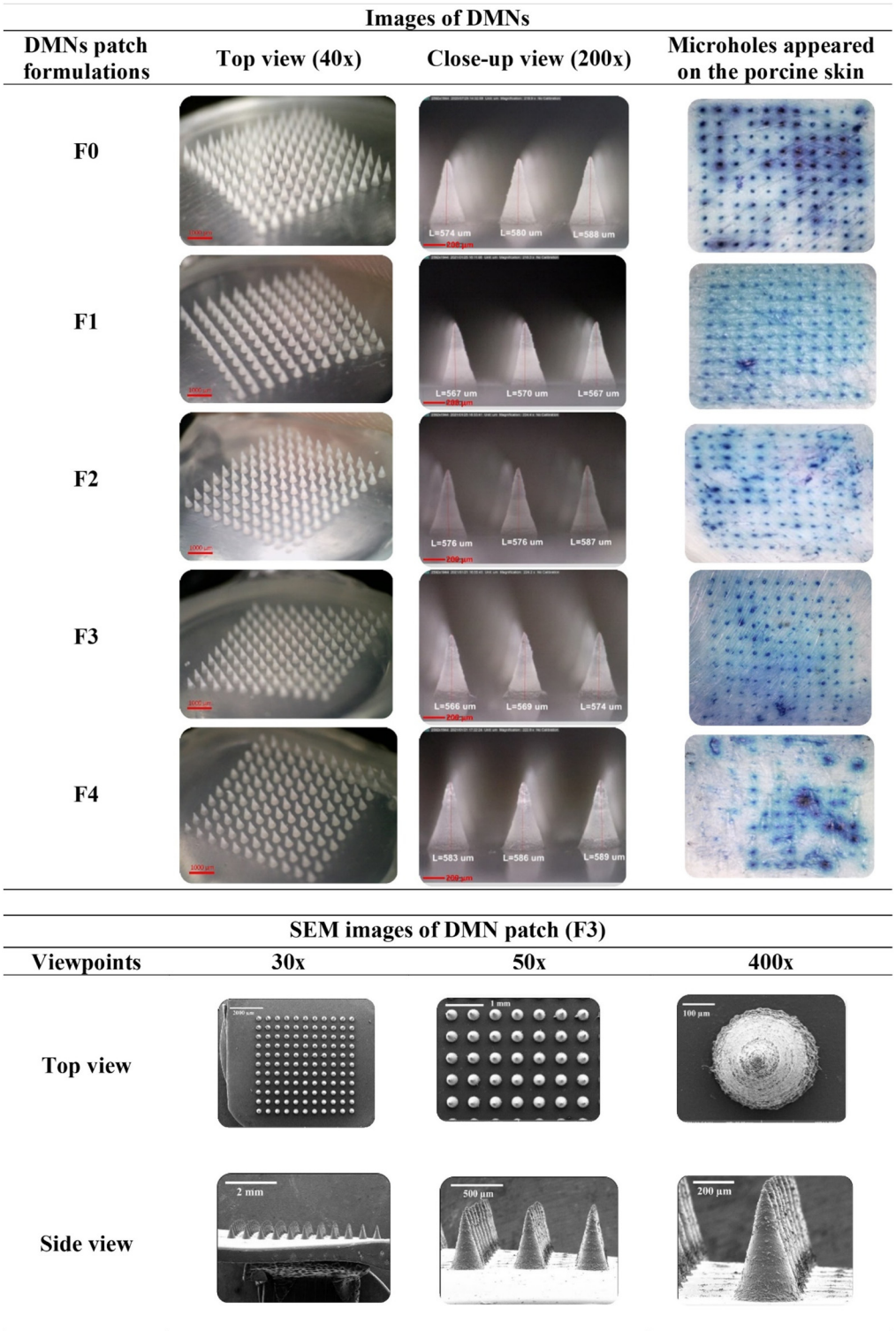

Fig. 3 Morphology of AA/Res-loaded DMN patches, stained microholes following insertion, and SEM images of 10% AA and 2% Res-loaded DMN patches (F3) from different viewpoints and at different magnifications.

patches to oppose compression and to evaluate the consistency of the patches from different batches produced in this study (Fig. 4A). The percentage reduction in the height of the patches ranged from 3 to 28%, depending on the compression forces applied. The percentage reduction in heights in all the formulations of DMN patches was gradually raised when the applied forces were increased. DMN patches with a higher drug loading showed a higher level of resistance to compression force. No base fractures or cracks of the DMNs were found during mechanical testing. The DMN patches resisted a compression force of 10.769 N per patch (0.089 N per needle), with heights decreased by only 12 to 19% for F1 to F4. According to Larrañeta *et al.*, this is the maximum force manually applied by the thumb press of a human.[42] The force–displacement curve of the DMN patches exhibited an initial increase in applied force with displacement. All DMN formulations did not show a distinct transition point during the test, indicating that the hard compression causes only progressive deformation of the DMNs (Fig. 4B). This result was in line with the percentage reduction in heights as F2–F4 revealed significant resistance to higher compression force compared to F0–F1. Hence, these DMN patches had sufficient mechanical strength for their intended use, demonstrated by the ability to maintain their height after opposing reasonable compression forces.

3.5.3 *Ex vivo* insertion study of DMN patches. Successful insertion of needles into the skin was confirmed using methylene blue staining.[42] The images presented in Fig. 3 show that more than 95% of microholes were created completely in the porcine skin after applying F0, F1, F2, and F3 DMN patches with a force of 10.769 N per patch for 30 s, as indicated by the number of stained microholes. However, only 54% of microholes (65 microholes) appeared when the F4 DMN patch was applied, owing to the high drug content which resulted in fragile needles. Therefore, the needles from the F4 DMN patches were not strong enough to penetrate the porcine skin.

3.5.4. Insertion depth of DMN patches. To confirm the insertion depth after applying selected F3 DMN patches, the number of holes created in each layer of the PF sheet was observed. Fig. s2.† shows the percentage of holes created in each PF layer after applying F3 DMN patches with a force of 10.769 N per patch for 30 s. The DMN patch was found to have pierced four layers of Parafilm that could reach an insertion depth of approximately 500 μm. This means that the application of MN arrays with an insertion force of 10.769 N per patch for 30 s, with the maximum force being manually applied by the thumb press of a human,[42] may be suitable for penetrating the skin.

3.5.5. Loading efficiency and loading capacity of DMN patches. The loading efficiency values of AA and Res were found to be 86 to 97% and 92 to 97%, respectively (Table 1). The loading capacity values of AA and Res in the DMN patches were 12 to 52% and 3 to 19%, respectively. The loading efficiency values of F2, F3, and F4 were within the acceptable range of percent drug loading (>90%).

3.6. *Ex vivo* and *in vivo* dissolution study of DMN patches

Microscopic analysis showed that the needle tips of unloaded DMN patches (F0) completely dissolved within 45 min (Fig. 5A). The 10% AA and 2% Res-loaded DMN patches (F3) completely dissolved within 15 min, both *ex vivo* and *in vivo*, as shown in Fig. 5B and C, respectively. The dissolution times in the *ex vivo* and *in vivo* tests were in line with the results reported by Aung *et al.*, which showed that drug-loaded DMN patches dissolved more quickly than unloaded DMN patches, as drugs incorporated into polymer mixtures enhanced the dissolution rate of DMN patches.[40] The types of polymers and drugs incorporated into the DMN patches affect the dissolution time. Interestingly, a comparison of *ex vivo* and *in vivo* dissolution times, as shown in Fig. 5B–D, and s2,† indicated that the DMN patches applied *in vivo* (live mice; Fig. 5C) had a lower dissolution time (5 to 15 min), compared to *ex vivo* appli-

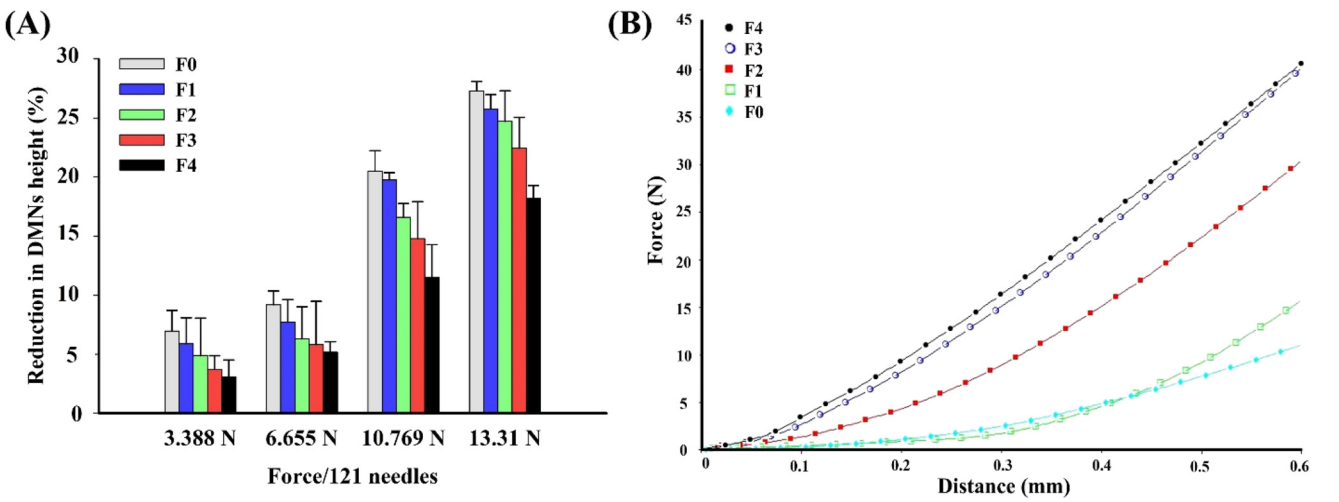

Fig. 4 (A) Percentage height reduction of F0, F1, F2, F3, and F4 DMN formulations following various compression forces applied (mean ± SD, n = 3). (B) Typical force–displacement curve of the compression force of different DMN formulations.

Table 1 Loading efficiency and loading capacity of F1, F2, F3, and F4 DMN patches

DMN patch formulations	Loading efficiency (%)		Loading capacity (%)	
	AA	Res	AA	Res
F1	86.57 ± 4.49	92.49 ± 2.76	12.04 ± 5.56	2.55 ± 0.02
F2	94.92 ± 4.58	94.64 ± 1.85	19.06 ± 1.39	7.15 ± 0.85
F3	95.19 ± 0.94	96.17 ± 2.88	36.76 ± 2.53	13.84 ± 2.09
F4	96.92 ± 1.40	97.04 ± 2.88	51.84 ± 1.63	18.74 ± 4.02

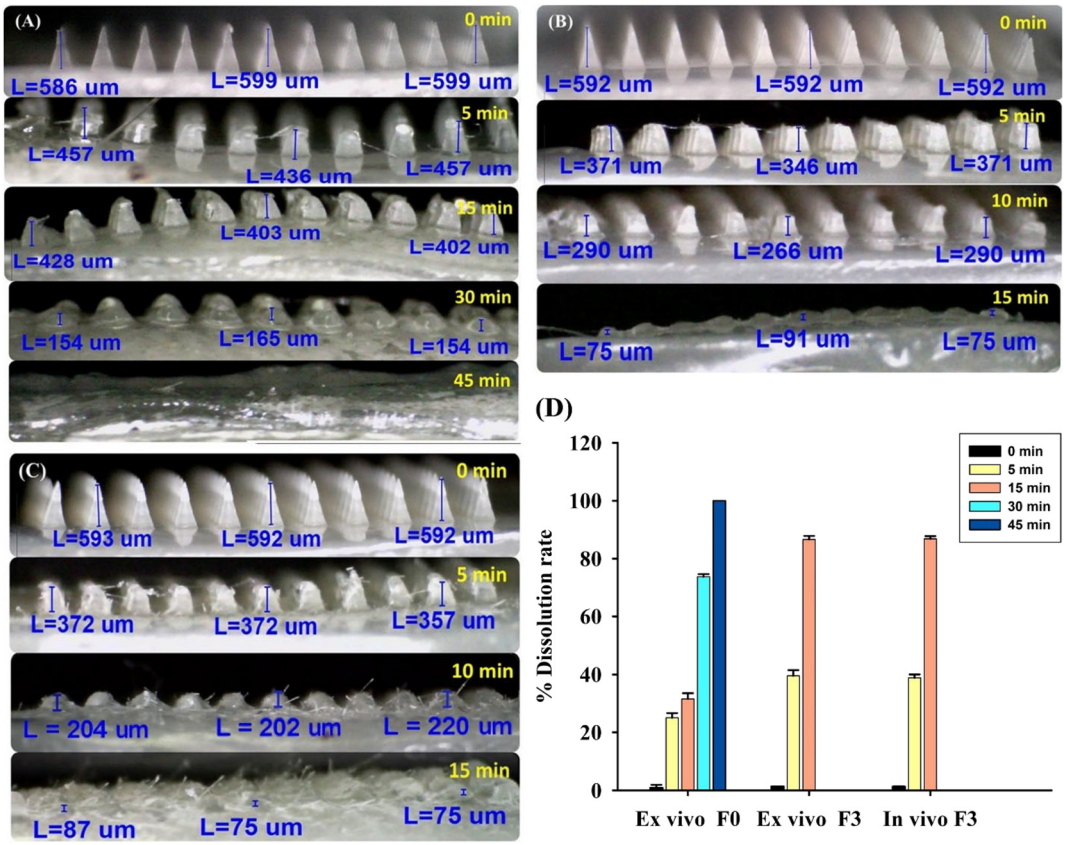

Fig. 5 *Ex vivo* dissolution images of DMN patches at different time points following application on neonatal porcine skin: (A) unloaded DMN (F0), (B) *ex vivo* dissolution of the AA/Res-loaded DMN patch (F3), (C) *in vivo* dissolution of the AA/Res-loaded DMN patch (F3), and (D) a histogram of the percentage dissolution rate of DMN patches.

cation (Fig. 5B). This is because the skin of live mice contains sufficient levels of interstitial fluid to absorb and solubilize the drugs. Therefore, results from *in vivo* tests have greater practical utility than those from *ex vivo* tests.

3.7. FTIR study

FTIR spectra from 4000 to 500 cm^{-1} of unloaded DMNs (fabricated from the PVP K-90 and Eudragit RL blend) and individual polymers (PVP K-90 and Eudragit RL) showed no peak differences (Fig. 6A), revealing that there was no interaction between the polymers in the DMN. However, comparing the FTIR spectra of unloaded and AA/Res-loaded DMNs showed a broad O–H stretching band in the 3700–3000 cm^{-1} region. This peak change represents hydrogen bonds between the polymers and AA or Res in the DMNs. Moreover, free OH groups (at 3700–3584 cm^{-1} of O–H stretching) were increased in DMNs loaded with AA and Res, leading to an increase in the dissolution time of the AA/Res-loaded DMNs compared to that of the unloaded DMNs.

3.8. Stability study of DMN patches

The DMN patches with 2% Res and 10% AA (F3) were stored for 6 months under sealed and unsealed conditions to evaluate their stability. The DMN patches revealed similar physical appearances (no change in color or appearance) after 6 months under both unsealed and sealed conditions. Fig. 6B shows that there was no significant change in the chemical stability of the patches that had been stored sealed or unsealed

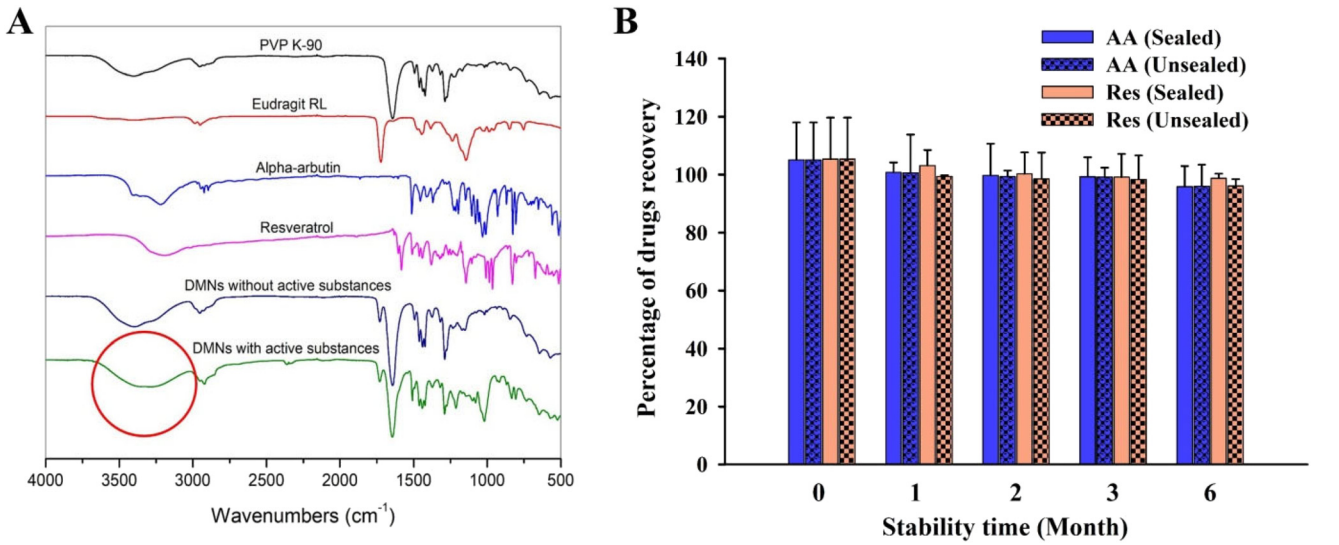

Fig. 6 (A) FTIR spectra in the range of 4000–500 cm^{-1} from PVP K-90 powder, Eudragit RL powder, AA powder, Res powder, unloaded DMNs, and AA/Res-loaded DMNs and (B) stability study of AA/Res-loaded DMN patches (F3) under sealed and unsealed conditions at 25 °C ± 2 °C and 60% ± 5% RH for 0, 1, 2, 3, and 6 months (mean ± SD, n = 3).

after 6 months, compared to day 0. The amount of AA recovered at 6 months was approximately 95.96% ± 7.44% in the unsealed packages and 95.77% ± 7.12% in the sealed packages, compared with the initial concentrations (103.01% ± 12.97%) (P > 0.05). The Res contents found in the DMN patches stored under unsealed and sealed conditions were 96.02% ± 1.62% and 98.65% ± 2.37%, respectively, compared with the initial concentrations (102.32% ± 14.35%). The results demonstrate that 2% Res and 10% AA incorporated into the Eudragit RL/PVP-K90 DMN patches remained physically and chemically stable after storage at 25 °C ± 2 °C and 60% ± 5% RH for 6 months, whether sealed or unsealed.

3.9. *In vitro* skin permeation of DMN patches

Fig. 7A and B show the permeation profiles of AA and Res delivered from the patches, physical mixtures, and cream formulations when applied across the excised full-thickness neonatal porcine skin. Over a 24 h period, the amounts of AA and Res permeated from the DMN patches were higher than those from the physical mixtures and cream formulations, except in the F1 formulation. Among all the formulations, superior transdermal delivery was observed in F3 (10% AA and 2% Res-loaded DMN patches), which delivered 1263.93 ± 123.21 μg cm^{-2} of AA (~1.89% of AA found in the patch and ~361.12% found in the needle tips) and 45.24 ± 4.23 μg cm^{-2} of Res (~0.34% of Res found in the patch and ~64.29% found in just the needles) across porcine skin. The F3 DMN patches showed significantly higher accumulation of AA and Res than the physical mixtures and cream formulations (approximately 30 times and 15 times higher, respectively). Accumulated AA and Res levels from the physical mixture were ~0.06% and ~0.02%, respectively. The levels of AA and Res accumulated from the cream formulations were ~0.13% and ~0.03%, respectively. In all DMN patch formulations except for F4, the amounts of AA and Res permeated increased when the drug concentrations increased. While in F4, there was a decline in drug permeation from 15% AA and 3% Res-loaded DMN patches.

The F3 DMN patches provided a significantly higher flux of both AA and Res compared with other formulations (F1, F2, F4, physical mixture, and cream) (P < 0.05), as shown in Fig. 7C. These observations indicated that drug permeation depended on the drug content in the formulations and the types of drug delivery systems.[54] Therefore, the F3 DMN patch formulation was selected as the optimal formulation for its excellent physical properties, including morphology, sharpness, mechanical strength, and skin insertion, resulting in high loading efficiency, loading capacity, skin permeation, and superior AA and Res delivery into the skin. Importantly, these provide evidence for the advantage of DMN patches over physical mixtures and cream formulations for improving transdermal drug delivery owing to their ability to penetrate the skin.[55]

3.10. Delivery of AA and Res into full-thickness neonatal porcine skin

At the end of the skin permeation experiment, the amount of AA and Res accumulated in the excised full-thickness neonatal porcine skin layers (thickness ~850 ± 120 μm) was studied to determine the amount of drug accumulation in the skin layer where melanocytes are located. As shown in Fig. 7D, the amounts of AA and Res in the skin layers delivered by the DMN patches were higher than those from the physical mixtures and cream formulations, which correlates with the *in vitro* skin permeation profile described above. Only small amounts of AA and Res were observed in the skin after the application of the physical mixtures and cream formulations. The F3 DMN patches significantly increased the amount of AA

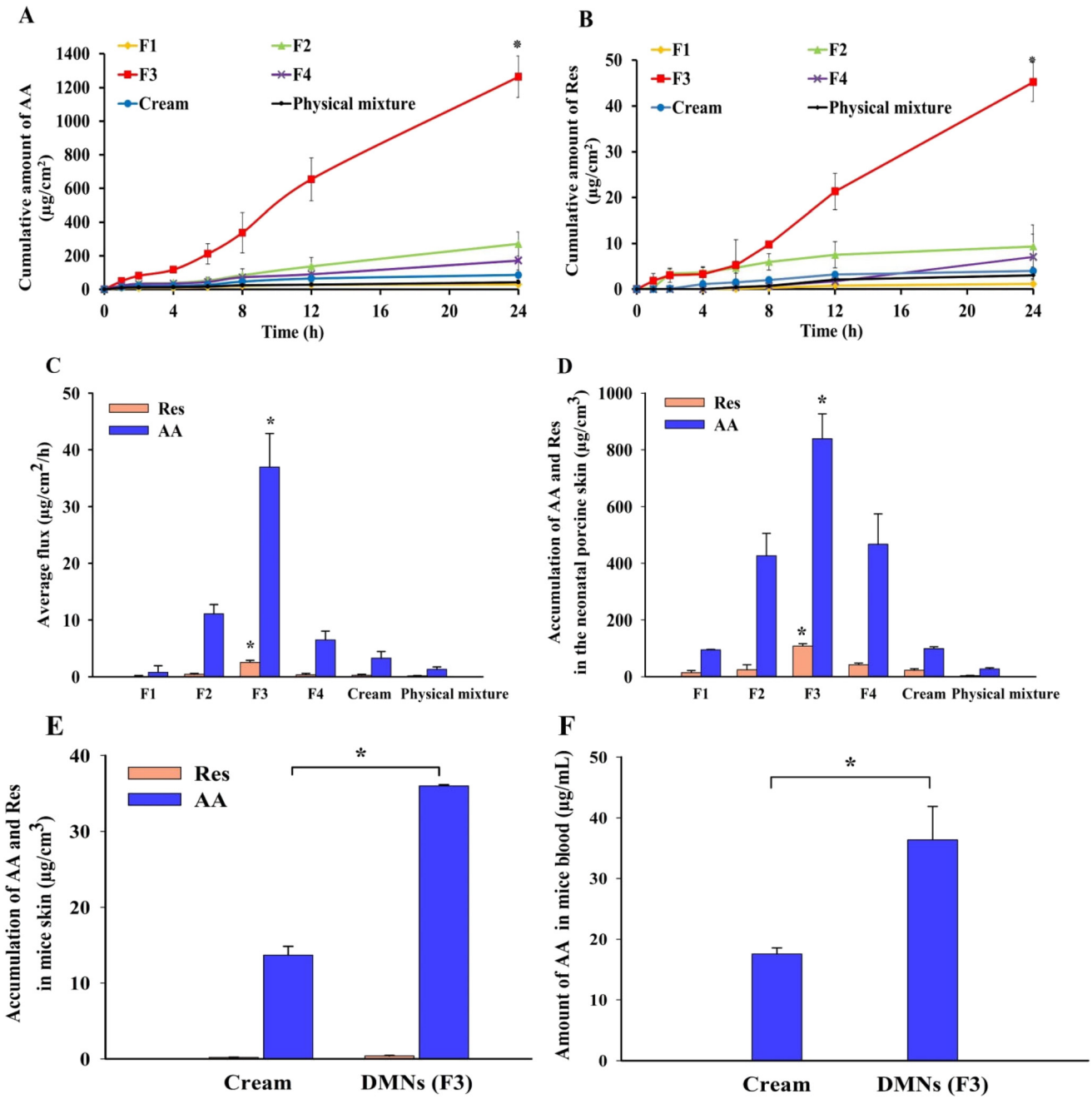

Fig. 7 *In vitro* skin permeation profiles of (A) AA, (B) Res, (C) average flux values, and (D) accumulation profiles of AA and Res in neonatal porcine skin treated with F1, F2, F3, and F4 DMN patches, cream formulations, and physical mixtures (mean ± SD, n = 3). *In vivo* profiles of (E) skin and (F) blood following the application of AA/Res-loaded DMN patches (F3) and cream (mean ± SD, n = 6) *Statistically significant ($P < 0.05$).

and Res accumulation in the skin ($P < 0.05$). The amount of AA delivered by the F3 DMN patch was 30.5 and 8.5 times higher than that provided by the physical mixture and the cream formulation, respectively. The amount of Res was increased by 28 times and 5 times in the DMN patch compared to that in the physical mixture and cream formulation, respectively.

The thickness of the epidermis in porcine skin ranged from ~30 to 140 μm, compared with ~50 to 120 μm found in human skin.[56] Hence, based on the findings of previous studies, we assumed that the stratum basale, where melanocytes are situated, is located at a depth of around 120–150 μm within the skin.[43,57] However, it is in the nature of mature melanocytes to form dendritic networks extending to the surrounding keratinocytes in the upper epidermis, where it determines skin color. Keratinocyte-derived paracrine factors stimulate melanocyte functions, including proliferation, differentiation, melanogenesis, and dendritogenesis. It is well known that Res effectively reduces UV damage in keratinocytes by inhibiting kerati-

nocyte-mediated indirect stimulation of melanocytes and reducing the production of inflammatory mediators to hinder inflammation-induced melanogenesis.[21,22] In human clinical trial studies by Jo *et al.* and Ryu *et al.*, it was found that using Res can enhance depigmentation after UV-induced tanning and can decrease hyperpigmented spots on the face ($P < 0.05$).[19,58] Therefore, delivery of AA and Res to the whole epidermis layer (at a depth of around 0 to 150 μm within the skin), where keratinocytes and melanocytes are located, would be beneficial for skin depigmentation. These results show that F3 DMN patches may successfully deliver AA and Res into the skin layer where melanocytes are situated.

3.11. *In vivo* study

The amount of AA and Res loaded into the DMN patch (F3) was approximately 67 mg and 13.4 mg (total amount in the baseplate and needles), or approximately 350 μg and 70 μg in just the needles. Over 24 h, the amount of AA delivered by the F3 DMN patch was 2.6 times higher than the amount delivered by the cream formulation. The amount of Res delivered by the F3 DMN patch was 1.9 times higher than the amount delivered by the cream formulation, as shown in Fig. 7E. These results correlate with a previous *in vitro* skin accumulation study which showed that AA and Res delivered by the DMN patch were retained in the skin to a greater extent than that delivered by cream formulations. The plasma concentration of AA analyzed by HPLC is illustrated in Fig. 7F. Only AA from the DMN patch and cream formulation reached the blood but at low levels. In contrast, the plasma Res concentration was not detected in the blood samples from any formulations. This might be due to the lipophilic nature of Res, allowing depot formation in the subcutaneous layer.

These demonstrate that the F3 DMN patches effectively penetrated into mouse skin and delivered the hydrophilic and hydrophobic cosmetic compounds into the target site for depigmentation. In concordance with the literature, accumulation of AA and Res at the site of melanin production and distribution was observed upon applying F3 DMN patches with the AA concentration below 1.0 mM. This suggests successful suppression of melanin content and tyrosinase activity without significantly affecting cell growth or tyrosinase mRNA levels in human melanoma cells.[59] Regarding the amount of drugs delivered, it seems that only the drugs from the needle shafts penetrated the skin, while none of the drugs from the baseplates were delivered, implying that the majority of the drugs remained in the patch itself. It is probable that there was insufficient interstitial fluid to solubilize the baseplate of the DMN patches within 24 h. Hence, AA and Res in the baseplates were unable to permeate into the skin in significant proportions.

3.12. *In vivo* skin resealing study

Skin resealing of the SC occurred within a reasonable timeframe and is presented in Fig. 8. At 2.5 h after withdrawal of the DMN patches, the blue microholes were imaged at designated time points (0, 1, 2, 4, 8, and 12 h). At the beginning of the experiment, the F3 DMN patches successfully penetrated the skin. Over time, mouse skin naturally resealed (~0%, 15%, 32%, 55%, 80%, and 100% at 0, 1, 2, 4, 8, and 12 h, respectively), as evidenced by microhole staining. These results indicate that following the application of a DMN patch, skin tissue could repair and restore spontaneously without leaving any permanent skin damage.[60] In addition, the application of 10% AA and 2% Res-loaded DMN patches for 2.5 h did not cause any injuries to mouse skin at the application site.

3.13. Human study

3.13.1. Characteristics of skin and safety. In order to prove the potential of DMNs to be translated into clinical practice, clinical studies are necessary. Fig. 9A and B show the forearm of a participant following the application of a 10% AA and 2% Res-loaded DMN patch (F3). The skin was smooth and clear before the application of the DMN patch (Fig. 9C). After application and removal of the DMNs, the patch area and microholes were visible on the skin, confirming that the microneedles had penetrated the skin (Fig. 9D). Within a period of 2 h after the DMN patch had been removed, the microneedle holes gradually disappeared and the skin returned to a normal appearance as shown in Fig. 9E. The application of DMN patches did not induce any signs of skin abnormalities or irritation at the application area in any of the healthy participants ($n = 15$) tested.

3.13.2. Skin melanin, skin erythema, skin hydration, skin elasticity, transepidermal water loss (TEWL), and safety assessment. Analysis of skin color (melanin and erythema), skin hydration, skin elasticity, and TEWL was performed using the DermaLab Combo® (Cortex Technologies, Denmark) to investigate whether any changes were caused to the skin as a result of the DMN application. Tests were carried out before (as a control) and after the application of the patches, as shown in Fig. 10A–E. Regarding skin color measurement using the DermaLab Combo® device, the analysis was based on narrow-

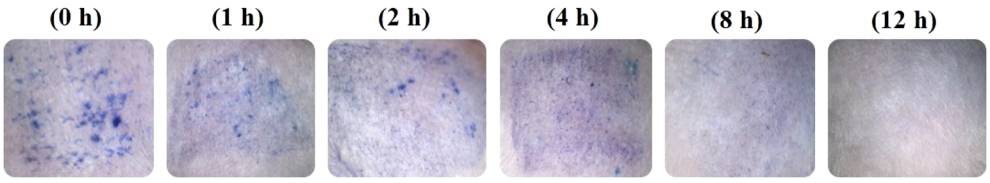

Fig. 8 *In vivo* skin resealing following removal of a DMN (F3) patch at various time points (0, 1, 2, 4, 8, and 12 h) after application.

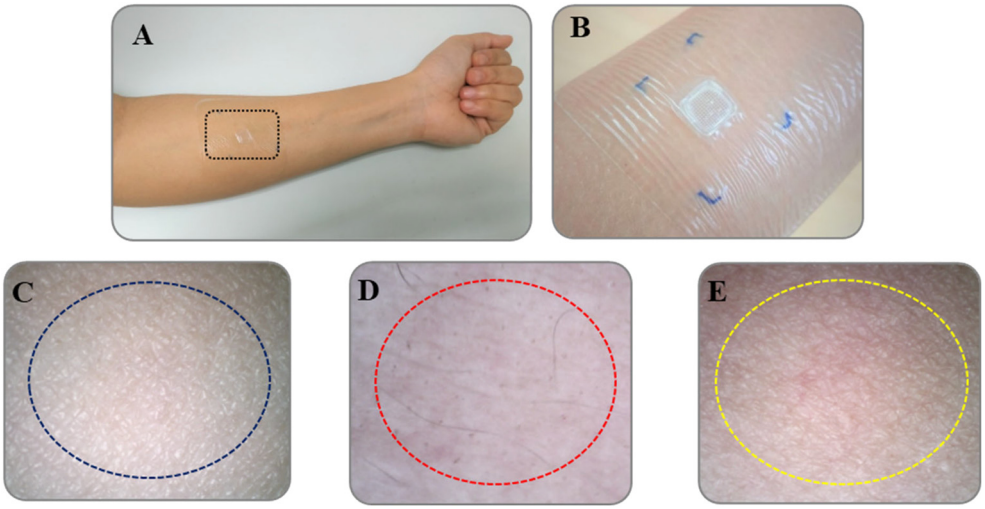

Fig. 9 The forearm of a healthy volunteer where an F3 DMN patch was applied. (A) A distant view (dotted black rectangle shows the area of DMN patch application) and (B) a close-up view and an area of DMN patch application in a volunteer (C) before application, (D) immediately after removal (following a 24 h period of application), and (E) 2 h after removal of the DMN patch (dashed lines refer to the applied area).

band reflectance spectrophotometry at a wavelength of 550 nm and 660 nm for erythema and melanin, respectively.[53,61] In the case of skin melanin, the amount of skin pigmentation recorded after a 24 h application of the DMN patches (93.89% melanin index relative to the normal skin measurements) was slightly decreased compared with that before the application (100% melanin index) (Fig. 10A). However, there was no significant difference in skin melanin before and after the DMN application. It is possible that wearing an AA/Res-loaded DMN patch just once for 24 h does not produce maximal skin lightening. Generally, it is necessary to use cosmetic products multiple times before the desired results can be achieved. Reports in the literature revealed that continuous AA or Res use for at least 4–12 weeks is necessary to observe skin lightening.[62–64] Thus, DMN patches should be used continuously for at least a month. Our study provided skin analysis and safety data, which may be a useful starting point in assessing the practical use of DMN patches before expanding the sample size to a full clinical trial.

Measurement of erythema (vascularity or the content of hemoglobin located deep in the dermis) is useful for determining skin reactions to irritants and allergens, typically seen as superficial redness as blood rushes to the skin surface.[65,66] Our results revealed that skin erythema slightly increased after the DMN patches had been applied for 24 h (108% erythema index), compared to that prior to the application (100% erythema index) (Fig. 10B). However, there was no significant difference in measurements before and after application. As seen in Fig. 9D, the skin area when the DMN patch was applied did not reveal a red appearance after removal, indicating the absence of any irritation or allergic reaction. It is likely that the DMN patch caused a slight rise in erythema due to changes in the perfusion of the dermal vasculature in response to the presence of foreign matter.

Skin hydration is a useful parameter to evaluate the moisture content of the skin. It is of importance in the cosmetic field and the treatment of many pathological skin diseases.[67] A high hydration level in the SC leads to higher skin capacitance. Therefore, a hydrated SC has higher electrical conductivity than a dehydrated SC.[68] The hydration probe of the DermaLab Combo® operates based on this concept and is the standard measurement of skin hydration. The average level of skin hydration in all volunteers slightly decreased ($P > 0.05$) after the DMN patches had been applied for 24 h (94.26% relative to normal skin) compared to that before the application (100%) (Fig. 10C). In the case of TEWL, the changes in TEWL were measured to evaluate the disruption of the skin water barrier function.[61,69] As shown in Fig. 10D, the TEWL values did not differ significantly before (6.42 ± 1.85 g mL^{-2} h^{-1}) and after the application of the DMN (6.78 ± 2.10 g mL^{-2} h^{-1}). The TEWL values in healthy skin using the DermaLab Combo® typically ranged from 1.10 to 21.40 g mL^{-2} h^{-1} (mean value = 6.48 ± 3.37 g mL^{-2} h^{-1}).[70] Although the application of DMN patches did not significantly affect SC hydration or water loss, the SC layer has been previously shown to lose some water content in order to dissolve the MNs.[71]

Skin elasticity was measured to determine whether any skin deformation took place. Measurements of elasticity in healthy skin are generally found to be between 2 and 15 MPa (with an average of about 6).[70,72] With respect to skin elasticity measurements, the length, volume, or shape of the skin is affected by the force applied that allows it to change and recover its shape when stretched or deformed.[73] The skin elasticity measurement system is designed to measure the modulus of elasticity by sucking the skin into the cavity using a vacuum probe. The higher the MPa, the greater the vacuum strength required to lift the skin.[72] As shown in Fig. 10E, there was no significant difference in the skin elasticity before and

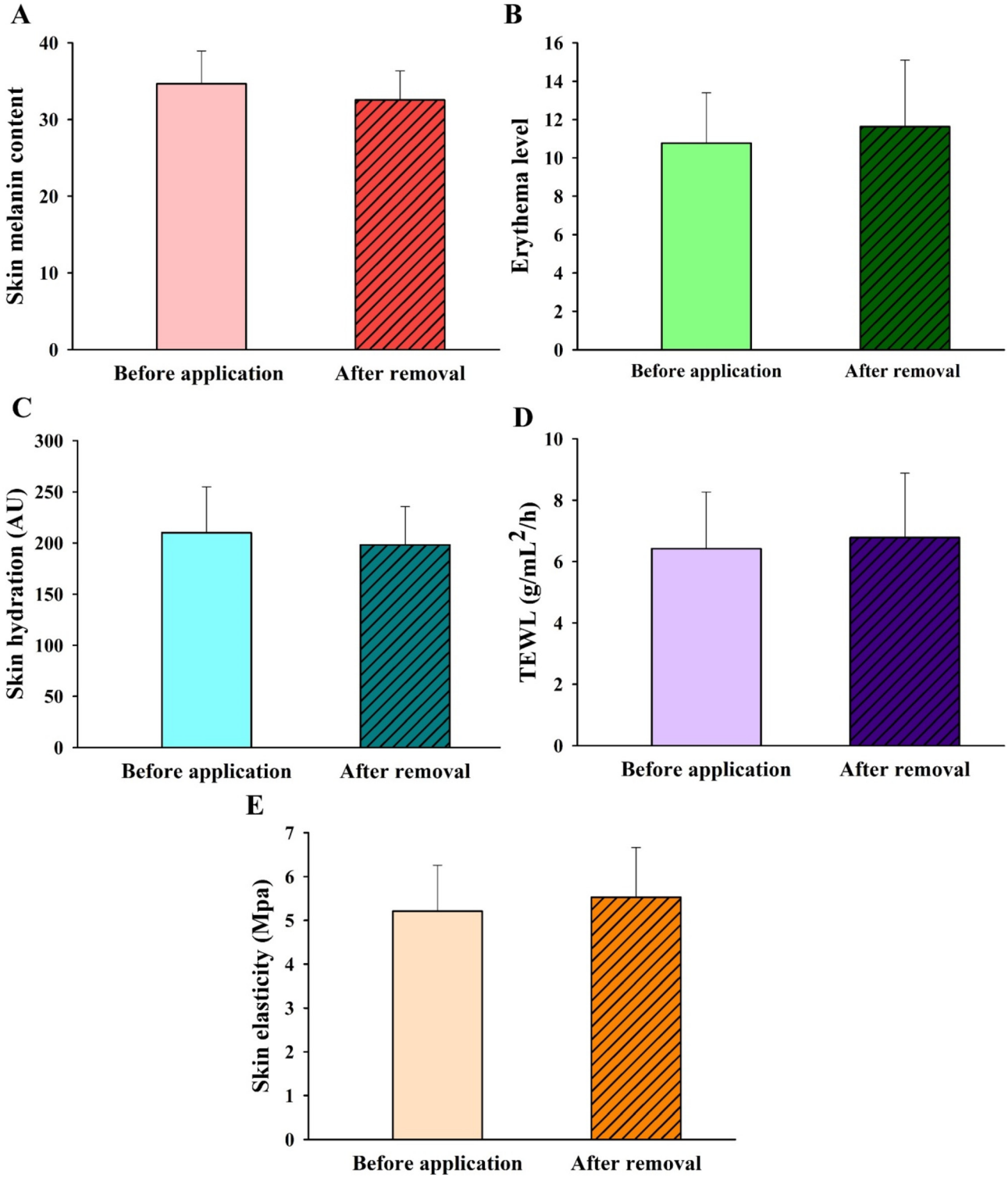

Fig. 10 Skin analysis of (A) skin melanin content, (B) erythema level, (C) skin hydration, (D) transepidermal water loss (TEWL), and (E) skin elasticity using the DermaLab® series (SkinLab Combo, Denmark) between before and after application of DMN patches in healthy human volunteers (mean ± SD, n = 15).

after the application of the DMN patches, suggesting that the skin can recover its original shape from any deformation that may arise after the application of DMNs. These observations correlate with Kalra *et al.* who reported that at a lower skin hydration level, the elasticity of the skin is increased due to hydrogen bond stretching, as water acts as a plasticizer that

increases elasticity.[71] In this clinical trial study, no significant differences were found in any of the parameters: skin melanin, skin erythema, skin hydration, TEWL, and skin elasticity, before and after the application of the F3 DMN patch. No skin hypersensitivity or irritation was reported from any of the participants throughout the clinical study. These suggest that DMN patches would be a safe platform for improving transdermal drug delivery.

To obtain a marked effect in lowering the melanin content of the skin and preventing inflammation-induced melanogenesis, active substances must reach effective concentrations at the target site of the epidermis layer, which is the location for melanin production and distribution. Therefore, penetration and retention of AA and Res in the skin are important for successful skin depigmentation. AA is known to exhibit low cutaneous absorption due to its high hydrophilicity.[64] In addition, Res is characterized as having chemical instability and poor aqueous solubility because of its high hydrophobicity, resulting in low permeation in the epidermis and transdermal.[2] This results in bioavailability of less than 1%.[74] Hence, the management of hyperpigmentation requires the repeated administration of a high dose of AA (56–80 mg per day, divided in two daily doses for at least 4 weeks, at a concentration of up to 5% or not more than 450 mg kg^{-1} day^{-1}).[10,75] It has been suggested that AA and Res have low efficacy at lowering the melanin content due to the poor penetration and solubility of the free drugs at the target site. This study suggests that DMN patches could be a promising delivery platform that could enhance skin depigmentation through AA and Res synergistic effects. The fabricated AA/Res-loaded DMN patch was able to overcome the SC barrier for transdermal delivery of AA and Res and maintain the compounds at the application site, allowing bioactivity in the target tissue with minimal systemic distribution.

Following absorption of interstitial fluid in the skin, the AA/Res-loaded DMN patches sufficiently dissolved to release the drugs. The needles were differentiated from the baseplate following removal, leaving the needles in the skin. The composited substances were then released from the needles and had penetrated the skin *via* diffusion. This composite swelled in the skin before gradually dissolving. The active compounds were then continuously released over several hours to a day. The hydrophilic nature of PVP-K90 and the hydrophobic properties of Eudragit RL 100 polymers produced suitable gels that decreased the hydrophilicity of AA and increased the hydrophilicity of Res. Because AA and Res incorporation in suitable polar/nonpolar polymers can considerably increase their permeation, the release and accumulation of the active substances into the skin and skin interstitial fluid may be further understood.[12,24,76] These findings have potential importance in improving the efficacy of using AA and Res by enhancing compound-related bioavailability, which is associated with topical administration with minimal systemic side effects. The drug from both delivery systems, the DMN patch and cream, reached the blood, but at acceptable concentrations, as can be seen in Fig. 10B. With regard to safety, the AA/Res-loaded DMN patches (F3) dissolved upon uptake by the interstitial fluid of human skin, thus preventing the onset of any skin hypersensitivity or irritation.

4. Conclusion

The findings presented here clearly show the potential of 10% AA and 2% Res-loaded DMN patches to deliver skin depigmentation agents into the skin layer containing melanocytes. This research demonstrates the advantages of MN technologies for improving the local administration of skin-lightening agents, which are limited due to their poor solubility and low percutaneous absorption. AA/Res-loaded DMN patches provide superior drug delivery for topical administration both *in vitro* and *in vivo*, as they can improve the delivery of cosmetic agents into the epidermis. Moreover, results from our human study also confirmed the safety of the DMNs, in which there were no skin hypersensitivity or irritation issues in any of the volunteers. This study highlights that DMN patches could be a promising platform for skin depigmentation. Their value in practical use is likely to be considered. Further clinical studies on the efficacy of AA/Res-loaded DMN patches over longer periods of application (at least 2–4 weeks) are still needed to confirm their efficacy for skin lightening and further commercialization.

Conflicts of interest

The authors report no conflicts of interest. The authors alone are responsible for the content and writing of this article.

Acknowledgements

This research was financially supported by the Office of the Permanent Secretary, Ministry of Higher Education, Science, Research and Innovation (grant no. RGNS 63–100), the National Research Council of Thailand (grant no. N42A650221 and N42A650551), and the Research and Creative Fund, Faculty of Pharmacy, Silpakorn University. We would like to thank Dr John Tigue for proofreading.

References

1 J. P. Ebanks, R. R. Wickett and R. E. Boissy, Mechanisms regulating skin pigmentation: the rise and fall of complexion coloration, *Int. J. Mol. Sci.*, 2009, **10**(9), 4066–4087.
2 S. Intagliata, *et al.*, Strategies to Improve Resveratrol Systemic and Topical Bioavailability: An Update, *Antioxidants*, 2019, **8**(8), 244.
3 I. Hwang and S. Hong, Neural Stem Cells and Its Derivatives as a New Material for Melanin Inhibition, *Int. J. Mol. Sci.*, 2018, **19**(1), 36.

4 A. Arbab and M. Eltahir, Review on Skin Whitening Agents, *Khartoum Pharm. J.*, 2010, **13**, 5–7.
5 J. W. Shin and K. C. Park, Current clinical use of depigmenting agents, *Dermatol. Sin.*, 2014, **32**(4), 205–210.
6 C. Couteau and L. Coiffard, Overview of Skin Whitening Agents: Drugs and Cosmetic Products, *Cosmetics*, 2016, **3**(3), 27.
7 Y. C. Boo, Arbutin as a Skin Depigmenting Agent with Antimelanogenic and Antioxidant Properties, *Antioxidants*, 2021, **10**(7), 1129.
8 E. Ephrem, H. Elaissari and H. Greige-Gerges, Improvement of skin whitening agents efficiency through encapsulation: Current state of knowledge, *Int. J. Pharm.*, 2017, **526**(1), 50–68.
9 P. Migas and M. Krauze-Baranowska, The significance of arbutin and its derivatives in therapy and cosmetics, *Phytochem. Lett.*, 2015, **13**, 35–40.
10 Scientific Committee on Consumer Safety and G. H. Degen, Opinion of the Scientific Committee on Consumer safety (SCCS) – Opinion on the safety of the use of α-arbutin in cosmetic products, *Regul. Toxicol. Pharmacol.*, 2016, **74**, 75–76.
11 J. Won and J. W. Park, Improvement of arbutin trans-epidermal delivery using radiofrequency microporation, *Trop. J. Pharm. Res.*, 2014, **13**, 1775–1781.
12 K. Robinson, C. Mock and D. Liang, Pre-formulation studies of resveratrol, *Drug Dev. Ind. Pharm.*, 2014, **41**, 1–6.
13 I. Gülçin, Antioxidant properties of resveratrol: A structure-activity insight, *Innovative Food Sci. Emerging Technol.*, 2010, **11**, 210–218.
14 J. Li, *et al.*, A comparative study of anti-aging properties and mechanism: resveratrol and caloric restriction, *Oncotarget*, 2017, **8**(39), 65717–65729.
15 M. Elshaer, *et al.*, Resveratrol: An overview of its anti-cancer mechanisms, *Life Sci.*, 2018, **207**, 340–349.
16 P. Shah and J. Patel, Resveratrol and its biological actions, *Int. J. Green Pharm.*, 2010, **4**, 15–21.
17 P. Devi, *et al.*, *Novel Drug Delivery Systems of Resveratrol to Bioavailability and Therapeutic Effects*, in *Resveratrol - Adding Life to Years, Not Adding Years to Life*, ed. F. A. Badria, IntechOpen, London, 2019.
18 Y. Wang, *et al.*, Synergistic Promotion on Tyrosinase Inhibition by Antioxidants, *Molecules*, 2018, **23**(1), 106.
19 D. Jo, *et al.*, Human skin-depigmenting effects of resveratryl triglycolate, a hybrid compound of resveratrol and glycolic acid, *Int. J. Cosmet. Sci.*, 2018, **40**(3), 256–262.
20 C. Lin, *et al.*, Modulation of Microphthalmia-associated Transcription FactorGene Expression Alters Skin Pigmentation, *J. Invest. Dermatol.*, 2003, **119**, 1330–1340.
21 R. Newton, *et al.*, Post-Transcriptional Regulation of Melanin Biosynthetic Enzymes by cAMP and Resveratrol in Human Melanocytes, *J. Invest. Dermatol.*, 2007, **127**, 2216–2227.
22 X. Wang and Y. Zhang, Resveratrol alleviates LPS-induced injury in human keratinocyte cell line HaCaT by up-regulation of miR-17, *Biochem. Biophys. Res. Commun.*, 2018, **501**(1), 106–112.
23 J.-I. Na, *et al.*, Resveratrol as a Multifunctional Topical Hypopigmenting Agent, *Int. J. Mol. Sci.*, 2019, **20**(4), 956.
24 G. Davidov-Pardo and D. McClements, Resveratrol Encapsulation: Designing Delivery Systems To Overcome Solubility, Stability And Bioavailability Issues, *Trends Food Sci. Technol.*, 2014, **38**(2), 88–103.
25 T. Pentek, *et al.*, Development of a Topical Resveratrol Formulation for Commercial Applications Using Dendrimer Nanotechnology, *Molecules*, 2017, **22**, 137.
26 E. Larrañeta, *et al.*, Microneedle arrays as transdermal and intradermal drug delivery systems: Materials science, manufacture and commercial development, *Mater. Sci. Eng., R*, 2016, **104**, 1–32.
27 Y. Park, *et al.*, Transdermal Delivery of Cosmetic Ingredients Using Dissolving Polymer Microneedle Arrays, *Biotechnol. Bioprocess Eng.*, 2015, **20**, 543–549.
28 R. Mahato, Chapter 13 - Microneedles in Drug Delivery, in *Emerging Nanotechnologies for Diagnostics, Drug Delivery and Medical Devices*, ed. A. K. Mitra, K. Cholkar and A. Mandal, Elsevier, Boston, 2017, pp. 331–353.
29 K. J. Lee, *et al.*, A Practical Guide to the Development of Microneedle Systems – in Clinical Trials or on the Market, *Int. J. Pharm.*, 2019, **573**, 118778.
30 K. van der Maaden, W. Jiskoot and J. Bouwstra, Microneedle Technologies for (Trans) Dermal Drug and Vaccine Delivery, *J. Controlled Release*, 2012, **161**, 645–655.
31 Y. Lee, *et al.*, Odorless Glutathione Microneedle Patches for Skin Whitening, *Pharmaceutics*, 2020, **12**(2), 100.
32 R. Wang, *et al.*, Transdermal delivery of allopurinol to acute hyperuricemic mice via polymer microneedles for the regulation of serum uric acid levels, *Biomater. Sci.*, 2023, **11**(5), 1704–1713.
33 Z. Zeng, *et al.*, Rational design of flexible microneedles coupled with CaO2@PDA-loaded nanofiber films for skin wound healing on diabetic rats, *Biomater. Sci.*, 2022, **10**(18), 5326–5339.
34 L. Ruan, *et al.*, Transdermal delivery of multifunctional CaO2@Mn-PDA nanoformulations by microneedles for NIR-induced synergistic therapy against skin melanoma, *Biomater. Sci.*, 2021, **9**(20), 6830–6841.
35 N. N. Aung, *et al.*, HPMC/PVP Dissolving Microneedles: a Promising Delivery Platform to Promote Trans-Epidermal Delivery of Alpha-Arbutin for Skin Lightening, *AAPS PharmSciTech*, 2019, **21**(1), 25.
36 X.-H. Yuan, *et al.*, Vasoactive intestinal peptide stimulates melanogenesis in B16F10 mouse melanoma cells via CREB/MITF/tyrosinase signaling, *Biochem. Biophys. Res. Commun.*, 2016, **477**, 336–342.
37 Y. J. Lim, *et al.*, Inhibitory effects of arbutin on melanin biosynthesis of alpha-melanocyte stimulating hormone-induced hyperpigmentation in cultured brownish guinea pig skin tissues, *Arch. Pharmacal Res.*, 2009, **32**(3), 367–373.
38 T.-C. Chou, Drug Combination Studies and Their Synergy Quantification Using the Chou-Talalay Method, *Cancer Res.*, 2010, **70**(2), 440.

39 W. Xu, W. W. Ma and H. H. Zeng, Synergistic effect of ethaselen and selenite treatment against A549 human non-small cell lung cancer cells, *Asian Pac. J. Cancer Prev.*, 2014, **15**(17), 7129–7135.
40 N. N. Aung, *et al.*, Enhancement of transdermal delivery of resveratrol using Eudragit and polyvinyl pyrrolidone-based dissolving microneedle patches, *J. Drug Delivery Sci. Technol.*, 2021, **61**, 102284.
41 K. M. El-Say, Maximizing the encapsulation efficiency and the bioavailability of controlled-release cetirizine microspheres using Draper-Lin small composite design, *Drug Des., Dev. Ther.*, 2016, **10**, 825–839.
42 E. Larrañeta, *et al.*, A Proposed Model Membrane and Test Method for Microneedle Insertion Studies, *Int. J. Pharm.*, 2014, **472**(1–2), 65–73.
43 B. Pamornpathomkul, *et al.*, Dissolving polymeric microneedle arrays for enhanced site-specific acyclovir delivery, *Eur. J. Pharm. Sci.*, 2018, **121**, 200–209.
44 N. N. Aung, *et al.*, Fabrication, characterization and comparison of α-arbutin loaded dissolving and hydrogel forming microneedles, *Int. J. Pharm.*, 2020, **586**, 119508.
45 B. Z. Chen, *et al.*, A basal-bolus insulin regimen integrated microneedle patch for intraday postprandial glucose control, *Sci. Adv.*, 2020, **6**(28), 583–595.
46 F. Cilurzo, P. Minghetti and C. Sinico, Newborn pig skin as model membrane in in vitro drug permeation studies: a technical note, *AAPS PharmSciTech*, 2007, **8**(4), 97–100.
47 E. Larrañeta, *et al.*, A proposed model membrane and test method for microneedle insertion studies, *Int. J. Pharm.*, 2014, **472**(1), 65–73.
48 H. Nguyen, *et al.*, Poly (vinyl alcohol) microneedles: Fabrication, characterization, and application for transdermal drug delivery of doxorubicin, *Eur. J. Pharm. Biopharm.*, 2018, **129**, 88–103.
49 Y. Chen, *et al.*, Fabrication of coated polymer microneedles for transdermal drug delivery, *J. Controlled Release*, 2017, **265**, 14–21.
50 K. Tansathien, *et al.*, Hair growth promoting effect of bioactive extract from deer antler velvet-loaded niosomes and microspicules serum, *Int. J. Pharm.*, 2021, **597**, 120352.
51 S. Kim, *et al.*, Enhanced Transdermal Delivery by Combined Application of Dissolving Microneedle Patch on Serum-Treated Skin, *Mol. Pharm.*, 2017, **14**(6), 2024–2031.
52 A. Quattrone, A. Czajka and S. Sibilla, Thermosensitive Hydrogel Mask Significantly Improves Skin Moisture and Skin Tone; Bilateral Clinical Trial, *Cosmetics*, 2017, **4**, 17.
53 T. Gankande, *et al.*, Interpretation of the DermaLab Combo® pigmentation and vascularity measurements in burn scar assessment: An exploratory analysis, *Burns*, 2015, **41**, 1176–1185.
54 C. H. Salamanca, *et al.*, Franz Diffusion Cell Approach for Pre-Formulation Characterisation of Ketoprofen Semi-Solid Dosage Forms, *Pharmaceutics*, 2018, **10**(3), 148.
55 E. Caffarel-Salvador, *et al.*, Potential of hydrogel-forming and dissolving microneedles for use in paediatric populations, *Int. J. Pharm.*, 2015, **489**(1), 158–169.
56 W. Meyer, R. Schwarz and K. Neurand, The skin of domestic mammals as a model for the human skin, with special reference to the domestic pig, *Curr. Probl. Dermatol.*, 1978, **7**, 39–52.
57 E. G. De Jalón, *et al.*, Topical application of acyclovir-loaded microparticles: quantification of the drug in porcine skin layers, *J. Controlled Release*, 2001, **75**(1), 191–197.
58 J. Ryu, *et al.*, A study of the human skin-whitening effects of resveratrol triacetate, *Arch. Dermatol. Res.*, 2015, **307**, 239–247.
59 K. Sugimoto, *et al.*, Inhibitory Effects of .ALPHA.-Arbutin on Melanin Synthesis in Cultured Human Melanoma Cells and a Three-Dimensional Human Skin Model, *Biol. Pharm. Bull.*, 2004, **27**, 510–514.
60 G. Grubauer, P. M. Elias and K. R. Feingold, Transepidermal water loss: the signal for recovery of barrier structure and function, *J. Lipid Res.*, 1989, **30**(3), 323–333.
61 C. Zhao, *et al.*, Variation of biophysical parameters of the skin with age, gender, and lifestyles, *J. Cosmet. Dermatol.*, 2021, **20**(1), 249–255.
62 Y. C. Boo, Human Skin Lightening Efficacy of Resveratrol and Its Analogs: From in Vitro Studies to Cosmetic Applications, *Antioxidants*, 2019, **8**, 332.
63 K. R. Patel, *et al.*, Clinical trials of resveratrol, *Ann. N. Y. Acad. Sci.*, 2011, **1215**, 161–169.
64 M. Saeedi, *et al.*, A comprehensive review of the therapeutic potential of α-arbutin, *Phytother. Res.*, 2021, **35**(8), 4136–4154.
65 K. Tansathien, *et al.*, Development of Sponge Microspicule Cream as a Transdermal Delivery System for Protein and Growth Factors from Deer Antler Velvet Extract, *Biol. Pharm. Bull.*, 2019, **42**(7), 1207–1215.
66 R. Abdlaty and Q. Fang, Skin erythema assessment techniques, *Clin. Dermatol.*, 2021, **39**(4), 591–604.
67 M. Milani and A. Sparavigna, The 24-hour skin hydration and barrier function effects of a hyaluronic 1%, glycerin 5%, and Centella asiatica stem cells extract moisturizing fluid: an intra-subject, randomized, assessor-blinded study, *Clin., Cosmet. Invest. Dermatol.*, 2017, **10**, 311–315.
68 M. Qassem, Review of Modern Techniques for the Assessment of Skin Hydration, *Cosmetics*, 2019, **6**, 19.
69 S. Marrakchi and H. Maibach, Biophysical parameters of skin: Map of human face, regional, and age-related differences, *Contact Dermatitis*, 2007, **57**, 28–34.
70 M. Anthonissen, *et al.*, Measurement of elasticity and transepidermal water loss rate of burn scars with the Dermalab (®), *Burns*, 2013, **39**, 420–428.
71 A. Kalra and A. Lowe, An Overview of Factors Affecting the Skins Youngs Modulus, *J. Aging Sci.*, 2016, **4**, 1–5.
72 C. Christ, *et al.*, Improvement in Skin Elasticity in the Treatment of Cellulite and Connective Tissue Weakness by Means of Extracorporeal Pulse Activation Therapy, *Aesthetic Surg. J.*, 2008, **28**(5), 538–544.

73 J. Everett and M. Sommers, Skin Viscoelasticity: Physiologic Mechanisms, Measurement Issues, and Application to Nursing Science, *Biol. Res. Nurs.*, 2013, **15**(3), 338–346.
74 T. Walle, Bioavailability of resveratrol, *Ann. N. Y. Acad. Sci.*, 2011, **1215**(1), 9–15.
75 A. Ratz-Łyko and J. Arct, Resveratrol as an active ingredient for cosmetic and dermatological applications: A review, *J. Cosmet. Laser Ther.*, 2018, **21**(2), 84–90.
76 N. Chandorkar, *et al.*, Alpha Arbutin as a Skin Lightening Agent: A Review, *Int. J. Pharm. Res.*, 2021, **13**, 3502–3510.